Biosonar signal propagation in the harbor porpoise's (*Phocoena phocoena*) head: The role of various structures in the formation of the vertical beam

Chong Wei[a)] and Whitlow W. L. Au
Hawaii Institute of Marine Biology, University of Hawaii, 46-007 Lilipuna Road, Kaneohe, Hawaii 96744, USA

Darlene R. Ketten
Department of Otology and Laryngology, Harvard Medical School, Biology Department, Woods Hole Oceanographic Institution, Woods Hole, Massachusetts 02543, USA

Zhongchang Song
College of Ocean and Earth Sciences, Xiamen University, Xiping Building, Xiangan South Road, Xiamen, 361100, People's Republic of China

Yu Zhang[b)]
Key Laboratory of Underwater Acoustic Communication and Marine Information Technology of the Ministry of Education, Xiamen University, Zengcuoan West Road, Xiamen, 361005, People's Republic of China

Harbor porpoises (*Phocoena phocoena*) use narrow band echolocation signals for detecting and locating prey and for spatial orientation. In this study, acoustic impedance values of tissues in the porpoise's head were calculated from computer tomography (CT) scan and the corresponding Hounsfield Units. A two-dimensional finite element model of the acoustic impedance was constructed based on CT scan data to simulate the acoustic propagation through the animal's head. The far field transmission beam pattern in the vertical plane and the waveforms of the receiving points around the forehead were compared with prior measurement results, the simulation results were qualitatively consistent with the measurement results. The role of the main structures in the head such as the air sacs, melon and skull in the acoustic propagation was investigated. The results showed that air sacs and skull are the major components to form the vertical beam. Additionally, both beam patterns and sound pressure of the sound waves through four positions deep inside the melon were demonstrated to show the role of the melon in the biosonar sound propagation processes in the vertical plane.

I. INTRODUCTION

Harbor porpoises are one of the smallest oceanic cetaceans living close to coastal areas or river estuaries. They use narrowband echolocation signals for detecting and locating prey and for spatial orientation. The characteristics of acoustic signals and the sound transmission in the harbor porpoise's biosonar system have been studied for decades (Møhl and Andersen, 1973; Kamminga and Wiersma, 1981; Hatakeyama and Soeda, 1990; Goodson *et al.*, 1995; Au *et al.*, 1999; Au *et al.*, 2006). The measurement results revealed that besides the difference in bandwidth, the echolocation signals of this species generally have more cycles

and longer duration than those of dolphins that use broadband echolocation signals. However, porpoises and dolphins seem to have a similar physical mechanism to excite vibration at the sound source. Harbor porpoises like many other odontocetes emit echolocation signals when pressurized air is forced through their phonic lips (Cranford *et al.*, 1996; Cranford *et al.*, 2014). The biosonar beam of harbor porpoises in the far field has been measured by different researchers (Au *et al.*, 1999; Au *et al.*, 2006; Koblitz *et al.*, 2012; Wisniewska *et al.*, 2012; Wisniewska *et al.*, 2015), and their results indicated that an echolocating harbor porpoise can generate a rapid series of pulses in a relatively narrow beam. How these animals produce such highly directed biosonar beams remains conjectural and the mechanisms that create such narrowband projected signals are still not well known.

Numerical acoustic models based on physics and mathematics can be used to gain further understanding of the acoustic processes of sound production and propagation in the head of dolphins and porpoises. Such numerical

---

[a)]Current address: Acoustic Research Laboratory, Tropical Marine Science Institute, National University of Singapore, 12A Kent Ridge Road, Singapore, 119222 Singapore

[b)]Also at State Key Laboratory of Acoustics, Institute of Acoustics, Chinese Academy of Sciences, Beijing 100190, People's Republic of China. Electronic mail: yuzhang@xmu.edu.cn

simulations are used to address questions that have been proven difficult to resolve experimentally. An accurate model requires high accuracy image reconstruction technology such as the computed tomography (CT) scan because the anatomical features in the animal's head are extremely complex. The numerical modeling has been used for investigating sound production, transmission and reception on different species of odontocetes, including short-beaked common dolphin (*Delphinus delphis*) (Aroyan *et al.*, 1992; Aroyan, 2001), Cuvier's beaked whale (*Ziphius cavirostris*) (Cranford, 2000), humpback whales (*Megaptera novaeangliae*) (Adam *et al.*, 2013), bottlenose dolphin (*Tursiops truncatus*) (Cranford *et al.*, 2014), baiji (*Lipotes vexillifer*) (Wei *et al.*, 2014; Wei *et al.*, 2016). However, the physiological mechanism of the biosonar beam formation in an echolocating harbor porpoise's head is still not well understood.

Some studies have suggested that the melon of odontocetes play a significant role on the biosonar beam formation based on the density and sound velocity gradient in the melon (Cranford, 1992; Karol *et al.*, 1978; Morris, 1986; Moore *et al.*, 2008). Kloepper *et al.* (2012) and Kloepper *et al.* (2015) suggested that changes in the beam were caused by changes in the shape of the melon affecting its focusing property. Thus, the melon focusing notion has been quite popular although it has never been shown that the gradient in impedance is sufficiently strong to cause sufficient ray bending to have the required focusing property. However, Aroyan *et al.* (1992) used a finite-difference method to simulate the biosonar beam formation in the head of a short-beaked common dolphin and found that the air sacs and skull were the dominant structures shaping the beam and the melon might be capable of mild focusing, but could not produce the dolphin's highly directed acoustic beam by itself. Au *et al.* (2010) experimentally measured the acoustic field on the forehead of echolocating Atlantic bottlenose dolphins with suction cup hydrophones that were placed on the side of the forehead and found the biosonar signals being directed (probably by the air sacs and skull) before the signals arrived at the melon. Wei *et al.* (2016) used a finite element model and a broadband transient signal at the source which more closely represented an echolocation dolphin than the study of Aroyan *et al.* (1992) which used a continuous tonal source. The numerical simulation results demonstrated that the melon in the baiji's head had only a slight influence on the shape and direction of its outgoing biosonar beam in the vertical plane. However, it seems that these results have not had much traction so the melon focusing hypothesis, although inaccurate, is still popular. Moreover, no studies have investigated the detailed role of the melon as the signals travel through this particular area in the animal's head. It would be impossible to conduct such experiments on the living animals, so using a numerical model to simulate the sound propagation processes in the animal's head is arguably the most effective approach to investigate how acoustic waves propagate through the dolphin and porpoise heads.

In this paper the finite element method was used to simulate the acoustic propagation through a harbor porpoise's head. The far field transmission beam pattern in the vertical plane and the waveforms of the receiving points around the forehead were compared with prior measurement results. The role of the main structures in the head such as the air sacs, melon and skull in the acoustic propagation was investigated. Additionally, both beam patterns and sound pressure of the sound waves through four positions deep inside the melon help clarify the role of the melon for sound traveling through it in the vertical plane.

II. METHODS

A. Acoustic properties of the head tissues

Numerical models require accurate geometric configuration reconstruction and physical property data acquisition of different tissues in the animal's head. Computed tomography (CT) scanned technology has been widely used for acquiring the two-dimensional and three-dimensional geometric configuration data (Aroyan *et al.*, 1992; Aroyan, 2001; Cranford *et al.*, 2014). The CT data of a harbor porpoise in this study were provided by Woods Hole Oceanographic Institution (WHOI) Biology Department. The specimen was immediately frozen to avoid decomposition after it died. A computed tomography scan of the carcass of the porpoise was conducted using a Siemens Volume Zoom CT scanner. A spiral protocol was employed with $120 \text{ kV} \times 320 \text{ mA}$ and 1 mm acquisitions. The animal was scanned in the prone position, head first with primary scans acquired in the transaxial plane. Images were reconstructed using soft tissue and ultra-high bone kernels. Raw attenuation data and all DICOM images were archived onto CD and magneto-optical disks. One of the slices from CT scan data in the sagittal cross section is shown in Fig. 1(a). Software Mimics 10.1 (Materialise, Belgium) was used to analyze the CT data and derive the Hounsfield Unit (HU) values of each structure in the harbor porpoise's head. Unfortunately, no tissue properties measurements were performed on this harbor porpoise. However, Wei *et al.* (2015) sliced a neonate Yangtze finless porpoise's head transversely across the body axis and measured the sound velocity and density of the soft tissues including the melon, blubber, muscle, mandibular fat, connective tissue. The HU values of the corresponding slices were obtained from high resolution computed tomography scanning data (the CT data were obtained on the next day after the animal died, so the specimen was very fresh). A univariate regression analysis was used to obtain the linear regression equations of HU with sound velocity and density. Then the distribution of HU values of all the structures was derived from CT data. On the basis of the HU distribution, the distributions of sound velocity and density of all the structures in the animal's head can be reconstructed (see more details in Wei *et al.*, 2015). The results were qualitatively consistent with the previous studies on Cuvier's beaked whale from Soldevilla *et al.* (2005) and Indo-pacific humpback dolphins from Wei *et al.* (2013). Since the mammalian tissue properties are conserved at the same temperature (Duck, 1990), The HU-to-sound velocity and HU-to-density relationships from Wei's measurement results (Wei *et al.*, 2015) were used in this study. The distributions of sound velocity, density, and acoustic impedance values of the different structures in the harbor porpoise's head including soft
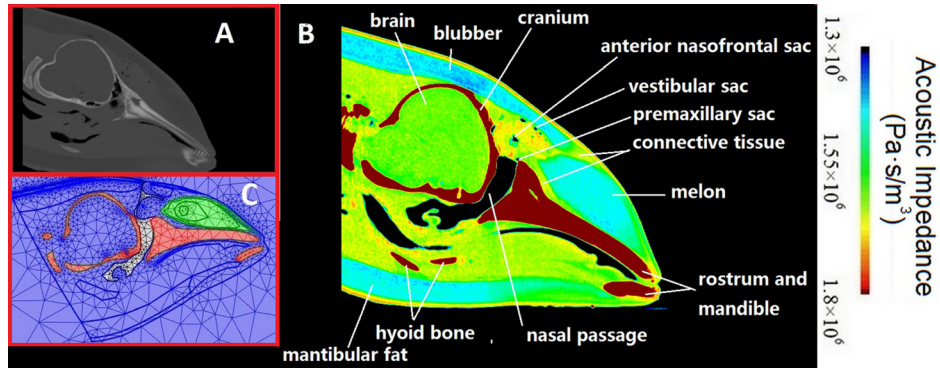
FIG. 1. (Color online) (a) One slice CT scan data of harbor porpoise's head in the sagittal cross section view. The gray level here represents the different HU values. (b) The distribution of the acoustic impedance of harbor porpoise's head. (c) The illustration of model mesh layout with reduced resolution in lateral view of the harbor porpoise's head (the elements with the original resolution would be too small to see).

tissues, bony structures, and air spaces were calculated based on the distribution of HU values derived from the CT data, shown as in Fig. 1(b). The air sacs in this specimen's head were partially inflated in the CT scan data. The precise shape of the air sacs for a live echolocating animal is not known and can only be approximated. Thus, the shape of the air sacs was adjusted to ensure they were in the proper positions based on the information provided by the prior studies (Cranford, 1988; Cranford et al., 1996; Nakamura et al., 1998; Huggenberger et al., 2009). The effects of the different volume of the air sacs on the resultant beam will be investigated in the future work. In order to quantify the potential effects of variations in tissue property in a certain range, a sensitivity analysis was applied in this model. The model was calculated multiple times while varying the sound velocity of the melon considering the acoustic property of animal's melon is inhomogeneous and the melon fills a large proportion of the forehead. The beam properties parameters from different results show that the potential effects of tissue property change across parameter ranges are limited in this model, more details can be found later in the discussion section.

The specimen involved in this research was an expired stranded animal. No live animals were obtained and no animal was harmed or killed for the purposes of this research. The processes for handling and examining the cadaveric specimens was reviewed and granted a blanket IACUC approval by the IACUC Animal Use Committee of the WHOI.

B. Modeling

The sound propagation processes in the harbor porpoise's head were simulated using a finite element model. A two-dimensional geometrical model of the animal's head with the size 25 cm length and 18 cm height was exported from the sagittal cross section of CT scan data. The length of the right side phonic lip at the coronal section is approximately 6 mm and can be showed at six sagittal slices based on the high resolution CT data (1 mm). The slice which is closest to the midline (about 6 mm) was chosen for building the numerical model. The model includes the following structures: melon, blubber, brain, musculature, mandibular

fat, connective tissue, bony structures, vestibular sac, nasal passage (including blowhole), premaxillary sac. Seawater surrounded the head to simulate the animal echolocating. COMSOL Multiphysics modeling software (Stockholm, Sweden) was used to run the numerical simulation in this study. The second-order triangle elements were used to free mesh the whole model and the elements size was set as at least ten elements per wavelength of the center frequency of the excitation signal at source ($\lambda = c_{water}/f_c$). The specimen was scanned in the prone position because the effect of gravity caused the angle between the rostrum and the table [see Fig. 1(a)], to be slightly different between a living and dead animal. Thus, the head was rotated slightly in the model so that the scan would more closely represent an echolocating porpoise [see Fig. 1(c)]. In order to simulate the porpoise echolocating in a large volume of water, the boundary of this model was represented by a perfectly absorbing space as an alternative to low-reflecting boundary (Bérenger, 1994). The model simulated the porpoise echolocating into an infinite water space.

The finite element computation was operated in time domain based on the physics of sound propagation in a fluid. The acoustic wave equation describing the transient acoustic phenomena in a stationary fluid can be written as

$$\frac{1}{\rho_0 c_s^2}\frac{\partial^2 p}{\partial t^2} + \nabla\left(-\frac{1}{\rho_0}\nabla p - \mathrm{q}_d\right) = Q_m, \qquad (1)$$

where ρ_0 denotes the equilibrium density (kg/m^3), c_s is the speed of sound (m/s), while q_d and Q_m are dipole and monopole sources, respectively (Wei et al., 2016; Song et al., 2016). The density ρ_0 and the speed of sound c_s can both be non-constant in space.

The pair of phonic lips are located on both left and right sides of the membranous nasal septum below the blowhole (Cranford et al., 1996). An exponentially damped sinusoid was used as a point sound source placed at one side of the phonic lip as shown in Fig. 2. It simulates the phonic lips opening and closing immediately by pressurized air causing the phonic lips to slam together and generate a short pulse. The pulse can be written as

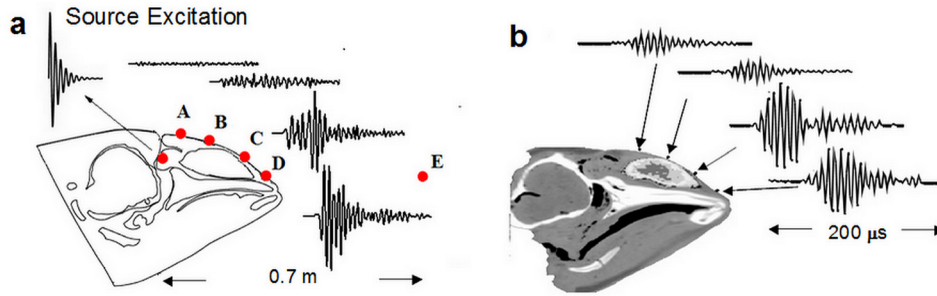J. Acoust. Soc. Am. **141** (6), June 2017

Wei et al.   4181

FIG. 2. (Color online) Comparison of the acoustic field on harbor porpoise's forehead between simulation and measurement. Points A–E are the receiving signals located in different positions. The position and the waveform of the source excitation were both showing in the figure. The amplitudes of the all the waveforms were relative to the highest amplitude. (a) Simulated results from this study. (b) Measurement results from Au *et al.* (2006).

$$Q_m = A \exp(\gamma t) \sin 2\pi f_0 t, \tag{2}$$

where γ is the damping rate, A is the pulse amplitude (m³/s), f_0 is the center frequency (Hz), and t is the time. According to the study by Au *et al.* (2006), the center frequencies of the harbor porpoise are between 120 and 130 kHz range. In order to be consistent with a real echolocating porpoise, a center frequency 130 kHz was used in this simulation.

III. RESULTS AND DICUSSIONS

Figure 2 shows the comparison of the acoustic field on the porpoise's forehead in the vertical plane between the simulation results of this study and the measurement results of Au *et al.* (2006). Four receiving points from A to D were set around the animal's forehead. The positions of these points were located approximately the same as the line configuration of the suction cup hydrophones used in the study by Au *et al.* (2006). Point E was a receiving point in the far field which was 0.7 m from the sound source at the main beam axis. The amplitudes of the all the output signals in Figs. 2(a) and 2(b) were relative to the highest amplitude at location D. The exponentially damped sinusoid was reflected by the complex structures in the animal's head when it traveled through the forehead of the porpoise. The reflected and direct signal components combined to form the waveform at each receiving point. The relative amplitudes of point C and point D were significantly higher than point A and point B, suggesting point C and D are closer to the main beam axis. Most of the energy in the signals was radiated into water at the anterior portion of the animal's forehead and very little energy was radiated to the top of the forehead. The simulated results were qualitatively consistent with the measurement result of Au *et al.* (2006). Moreover, the amplitude of the signal at point A was lowest even though it was located closest to the phonic lips. The results suggested that there was a highly directional beam formed in the animal's forehead even before it traveled through melon and were consistent with the result of Au *et al.* (2010).

The waveforms of both the simulated signal (point E) and the measured signal in the far field are shown in the Fig. 3 along with the spectra of both signals. The cross-correlation coefficient between the two signals was 0.65. The duration and the waveform of the measured signal and the simulated signal were very close, approximately at 160 μs.

The peak frequency of the simulated signal was 130 kHz, approximately 10 kHz higher than that of the measured signal. The 3 dB bandwidths of two signals were both within 10–15 kHz. According to the study by Au *et al.* (1999), harbor porpoises emit echolocation signals with peak frequencies between 125 and 130 kHz most often, with 3 dB bandwidths between 15 and 25 kHz. Figure 3 shows that the simulated signal in the far field in this study was a typical narrowband echolocation signal of the harbor porpoise.

The beam pattern in the vertical plane of this study was compared with the measured results of Au *et al.* (1999) and Koblitz *et al.* (2012) as shown in Fig. 4. The angle of the main beam from this study was close to the result measured by Koblitz *et al.* (2012). Both results were approximately 5° lower than the result measured by Au *et al.* (1999). Additionally, the 3 dB beamwidth from this study was 10.6°, which was close to the results from Koblitz *et al.* (2012) at 10.7°, and was lower than 16.5° of the measurements by Au *et al.* (1999).

According to the study by Au *et al.* (1999), the 3 dB beamwidth and directivity index of the biosonar beam of four different odontocete species are related to the ratio of the head diameter measured at the blowhole over the wavelength corresponding to the peak frequency. In order to compare the properties of the beam from simulation in this study with the results measured from actual animals of different species, the directivity index (DI) and 3 dB beamwidth were calculated. The horizontal and vertical beam widths of the
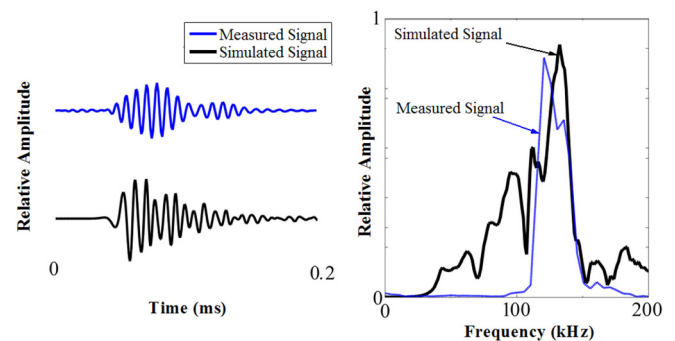

FIG. 3. (Color online) Comparison of both the simulated and measured (Au *et al.,* 1999) waveform and FFT results at the receiving points in the far field. The signal above in the left figure represents the measured signal and the signal below in the left figure represents the simulated signal. The waveforms are showing on the left and the results of Fast Fourier Transform are showing on the right.
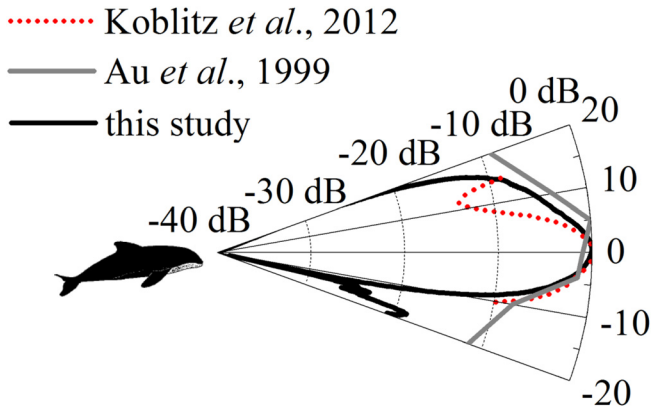
FIG. 4. (Color online) Comparison with the beam patterns results in the far field from simulated results in this study and the results measured by Au et al. (1999) and Koblitz et al. (2012). The dashed line represents the result from Koblitz et al. (2012), the gray line represents the result from Au et al. (1999) and the solid black line represents the result from the simulation results in this study.
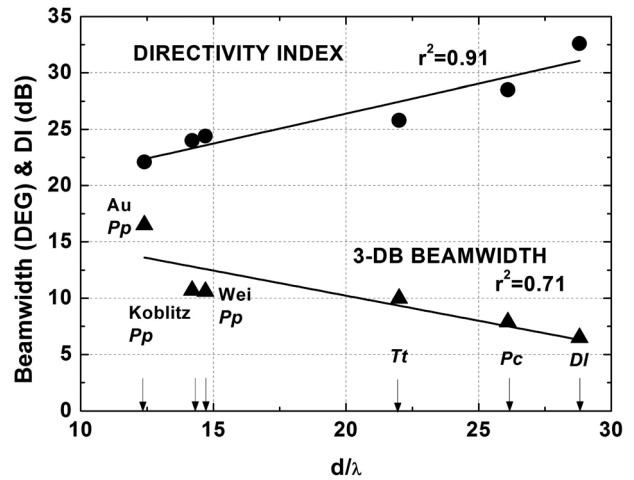

FIG. 5. The 3 dB beamwidth and directivity index from this study (Wei Pp) in comparison with the measurement results of four odontocete species. The four species are harbor porpoise, *Phocoena phocoena* ["Au pp" represents the results measured by Au et al. (1999), "Koblitz pp" represents the results measured by Koblitz et al. (2012)], bottlenose dolphin, *Tursiops truncatus* (Tt) (Au, 1993), false killer whale, *Pseudorca crassidens* (Pc) (Au et al., 1995), and beluga, *Delphinapterus leucas* (Dl) (Au, 1993).

harbor porpoise were assumed to be approximately the same (10.6°) according to the results on *Phocoena, Tursiops truncates*, and *Delphinapterus leucas* by Au (1993). The directivity index can be estimated by using a circular piston in a baffle to model the beam of the harbor porpoise. The directivity index for a circular piston can be expressed as a function of the 3 dB beamwidth (θ_{bw}) by the following equations (Au et al., 1999, Au and Hastings, 2008):

$$di = \left[\frac{0.509\,\pi}{\sin(\theta_{bw}/2)}\right]^2 \tag{3}$$

$$DI = 10\log(di). \tag{4}$$

In this study, the diameter of the harbor porpoise's head at the blowhole was approximately 0.168 m and the wavelength of the acoustic signal at 130 kHz was 0.0114 m so that d/λ ≈ 14.7. When the 3 dB beamwidth is 10.6°, DI can be calculated as 24.4 dB. The 3 dB beamwidth and directivity index estimated for the harbor porpoise's model are shown in Fig. 5. The values of r^2 for the regression of directivity index and 3 dB beamwidth with the ratio of the diameter of the odontocete head to the peak frequency of its echolocation signal are 0.91 and 0.71, respectively. The results from the simulation in this study were consistent with the curve-fit relating to measurements from actual animals of the same species but different individuals and with different species, suggesting that this model is reliable.

In order to investigate the role of the air sacs, melon and skull on the formation of the biosonar beam in an echolocating harbor porpoise, the acoustic pressure distributions in the far field for four cases were considered and the results are shown in Fig. 6. Air sacs, skull and melon were replaced by the surrounding soft tissue in case I, case II, and case III, respectively. Case IV simulated an actual echolocating harbor porpoise with the full head on the vertical plane which included the skull, melon, air sacs, connective tissue, blubber, musculature, mandibular fat, etc.
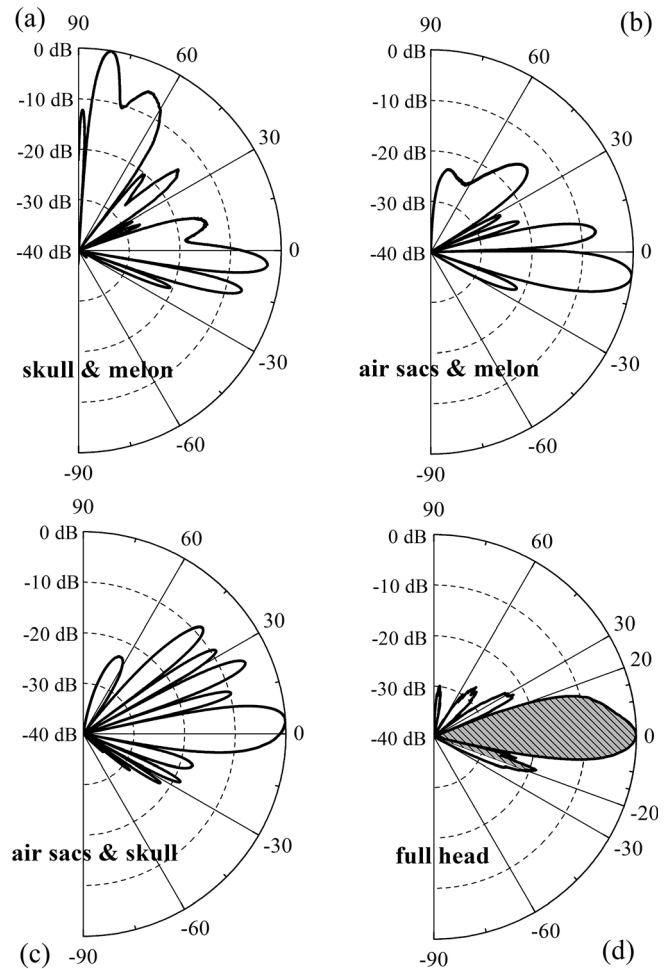

FIG. 6. The polar plots in the vertical plane of four cases. (a) Case I: skull plus melon with air sacs removed; (b) case II: air sacs plus melon with only skull removed; (c) case III: air sacs plus skull with only melon removed; and (d) case IV: the full head which includes the skull, melon, air sacs, connective tissue, blubber, musculature, mandibular fat etc. The area filled with the slanted lines is the same area in Fig. 4 from −20° to 20°.

J. Acoust. Soc. Am. **141** (6), June 2017

Wei et al. 4183

From the polar plot of case I with only the air sacs removed, there are more side lobes than in the other cases, and part of the energy in the beam propagates to the top and rear, indicating the air sacs act as acoustic reflectors to reduce side lobes and also to produce forward-propagating waves. In case II with the skull removed, the waves propagate in directions below the angle of the rostrum, suggesting that the skull (when present) reflects waves upward from the surface of the rostrum. Compared with the other cases, the main beam in case III with only the melon removed is relatively close to that of the full head case, but more side lobes are observed.

The results in Fig. 6 showed that a circular wave from the source point transforms into a directional beam by destructive and constructive interference by the air sacs (forward-reflecting) and skull (reflecting upward from the rostrum). In order to examine the role of the melon, two cases were used to show the wave propagation process deep inside the melon. The inhomogeneous melon was replaced by a homogeneous melon with the acoustic properties of the homogeneous melon being the same as that of the surrounding tissues. This case was used to compare with the full head case with the inhomogeneous melon. There were four positions from A to D set in the animal's melon in two cases, representing the waves just arrived at the melon, the waves travelled through one third of the melon, the waves travelled through half of the melon, and the waves left the melon. The specific changes of the waves when they travelled through the four positions are shown in Fig. 7. The beam pattern was plotted by determining the peak-to-peak sound pressure of a single click spreading from the source over a circle of radius equal to the distance from the source to the position indicated by the arrows. As shown in Fig. 7(a) the acoustic intensity, the beam width, and the angle of the main beam in

two cases at position A are very close, indicating the waves barely changed with or without the melon when they first arrive at the melon. The angle of the main beam in the full head case gradually goes higher than the one without the melon as the waves propagate further inside the melon. As the wave traveled from positions B to D, the wave for the full head began to bend while the beam pattern hardly changed. The 3 dB beamwidth of the two beams hardly changed when the waves traveled through the melon. In Fig. 7(d), the angle of the main beam in the full head case is approximately 3.5° higher than the case without the melon as the waves exited the melon. These results suggest that the direction of the porpoise's biosonar beam changes slightly as the signal travels through the melon.

Sound velocity of tissue is temperature dependent, and the sound velocity values from Wei et al. (2015) were measured at 23 °C, which is below the temperature of the melon in a living animal's head. The melon is vascularized, which has been hypothesized to be related to its thermoregulation by Houser et al. (2004). Such potential effect on tissue properties would add some extent of uncertainty to the model predictions, in order to quantify the uncertainty in the model and demonstrate how much the model output would have changed with potential range of sound velocity, the sound velocity of the melon was calculated at 23 °C, 27 °C, 32 °C, 37 °C according to the relationship between temperature and sound velocity measured by Song et al. (2017). In the study by Song et al. (2017), the relationship between the soft tissue's sound velocity and temperature demonstrated the nonlinearity of responses to temperature. The distribution of sound velocity of the melon at 23 °C, 27 °C, 32 °C, 37 °C can be estimated. The values of the 3 dB beamwidth and the angle of the main beam were collected using different sound velocity values of the melon in the simulations. The results
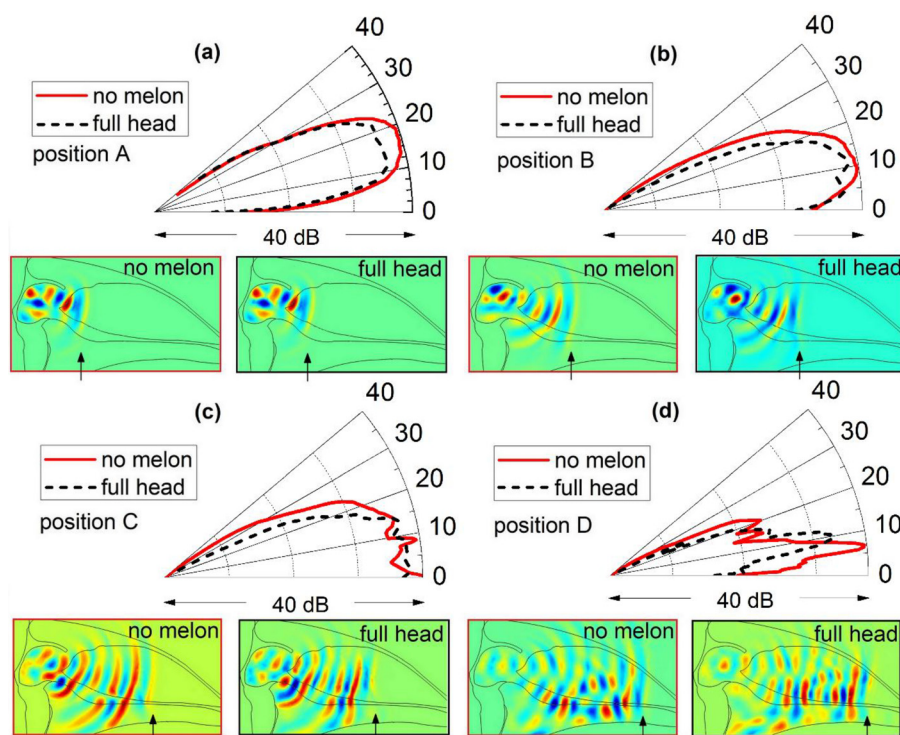

FIG. 7. (Color online) Comparison of the sound propagation processes deep inside the melons in two cases. The solid lines represent the case with only the removed melon and the dashed lines represent the full head model. The arrows show the four positions, A to D, which represent when the waves arrive at different locations in the melon: the waves just arrive at the melon, the waves travel through one third of the melon, the waves travel through half of the melon, and the waves leave the melon, respectively.

indicated that there was very little change in beam properties as shown in Table I suggesting that the output of this model is quantitatively consistent with the melon of a living animal and that the melon has the ability to thermoregulate.

The biological structures in the animal's head are composed of intermixed fluids and elastic solids. Only longitudinal waves exist in fluids, soft tissues, air spaces and water, while shear waves can be induced in solids such as the bony structures. However, much of the skull surface in the region of the animal's nasal passages is covered by air sacs and there is a huge mismatch between the acoustic impedance of the rostrum and surrounding soft tissues, so that the shear wave energy generated by a soft tissue sound source can be considered as limited (Aroyan et al., 1992). Therefore, it is sufficient to apply the pressure wave component to describe the acoustic field property in the fluid in this model. The results showed certain agreement to the measurement results. However, the influence of shear wave to the animal's acoustic processes will be tested and quantified by using several models of different species in future work.

The 3 dB beamwidth in the far field in this paper is 10.6°, which is close to the one measured by Koblitz et al. (2012) but is lower than the one measured by Au et al. (1999). The main reason is the difference in the size of the animals' heads. The diameter at the blowhole of the harbor porpoise used in our simulation was approximately 16.8 cm which is close to the diameter of approximately 16.2 cm for the porpoise used by Koblitz et al. (2012). Both of these two animals' head sizes are larger than the 14.8 cm for the porpoise used in the measurement of Au et al. (1999). The width of beam pattern is inversely proportional to the size of an animal's head, and the results shown in Fig. 5 reflect this relationship for three species of larger dolphins (*Tursiops truncatus*, *Pseudorca crassidens*, and *Delphinapterus leucas*) and three different *Phocoena phocoena*.

Previous studies have used numerical models and experimental measurements to display that the internal structures in the dolphin's head such as the air sacs, melon and skull contribute to the formation of biosonar beam (Aroyan et al., 1992; Houser et al., 2004; Au et al., 2010; Cranford et al., 2014; Finneran et al., 2014; Wei et al., 2014; Song et al., 2016; Wei et al., 2016). Aroyan et al. (1992) suggested that the air sacs and skull were the dominant factors in shaping the beam and the melon might be capable of mild focusing in the formation of the short-beaked common dolphin's biosonar beam. Finneran et al. (2014) demonstrated the reflective nature of the skull, specifically the premaxillary bones. A vibroacoustic finite element model was employed in

Cranford et al. (2014) to report the air spaces and the shape of the skull played important roles in the formation of the sound transmission beam in the bottlenose dolphin's head. Wei et al. (2016) used a broadband transit signal as the driving source to model the propagation of the echolocation clicks in the baiji's head, indicating that the air sacs and skull were the major contributor to the formation of the baiji's biosonar beam in vertical plane. The results shown in this paper are in line with the prior studies to report that the air sac and skull are the major components to form the harbor porpoise's vertical beam. If we compare case II with only the skull removed to the corresponding case in the baiji's model, the role of the skull in the baiji's head is bigger than in the harbor porpoise's head. The main reason might be the differences between the head shape of the harbor porpoise and the baiji; the rostrum of the baiji is longer than that of a harbor porpoise and a longer rostrum could provide more and better reflection in forming the beam.

Au et al. (2010) measured the acoustic field of the bottlenose dolphin's forehead and suggested that the beam was first formed by reflections off the air sacs and then refined by the sounds propagating through the melon. The results from this study with the sound propagation process inside the melon provide the first visual evidences to show that the vertical beam has already been significantly formed mainly by the air sacs and skull, and made slightly narrower by refractions in the connective tissue before it travels through the melon (see Fig. 7). These results are consistent with the results of Au et al. (2010). The graded acoustic impedance profile of the melon guides the waves along its inner core with the lowest acoustic impedance and slightly changes the angle of the main beam as the waves travel through it (see Fig. 7) and reduces the side lobes (see Fig. 6). Therefore, the melon functions mainly as an acoustic waveguide and also provides slight narrowing of the resultant biosonar beam.

Our results do not support the conclusions from Kloepper et al. (2012) and Kloepper et al. (2015), which suggested adaptive focusing of the echolocation beam and hypothesized that the deformation of the melon causes the biosonar beam to focus. They depicted the melon as an acoustic lens analogous to an optical lens. There has been new evidences to prove that the animals' biosonar beams are actually not focused in a way suggested by Kloepper et al. (2012) and Kloepper et al. (2015). The recent work by Finneran et al. (2016) demonstrated that focusing was not occurring through high-resolution measurements of the dolphin sonar beam and explained that apparent contradictions between the conclusion from Finneran et al. (2016) and the conclusions from Kloepper et al. (2012) and Kloepper et al. (2015) were likely the result of a misinterpretation of data rather than a difference in biosonar emissions across species. The term "focus" means there is a sign of converging behavior during sound propagation, the odontocetes biosonar beams are directional but not actually focused (converging wave fronts), the term focus is sometimes erroneously used when collimation is meant. The numerical evidences from the modeling in this study (Fig. 7) showed the angle of main beam changed when the melon was present, strongly suggesting the collimation of the outgoing signals. Using

TABLE I. Comparison of the angle of main beam and 3 dB beamwidth from the models using different sound velocity values of melon.

Temperature (°C)	23	27	32	37
The sound velocity of melon (m/s)	1365–1502	1331–1468	1313–1450	1249–1386
The angle of main beam (°)	0.5	−0.7	1.7	0.3
3 dB beamwidth (°)	10.6	10.5	10.4	10.6

"collimation" to describe the role of melon during the biosonar emission instead of using "focusing" would be more precise. Thus, the popular melon focusing notion is not accurate. Second, with respect to the hypothesis mentioned by Kloepper *et al.* (2012) and Kloepper *et al.* (2015), although the recent data reported the biosonar beam property can be changed by the deformation of animal's forehead (Wisniewska *et al.*, 2015), there could be many factors involved in this complex process (not only by the deformation of melon). The deformation is caused by the action of fibers and tendons of the muscles associated with the melon and it would also alter the shape of other soft tissues in animal's forehead such as the connective tissue. Even if the melon undergoes small changes in shape, the gradients in the impedance will not change much so that very minor effects will take place. The deformation of the forehead could also change the position of the phonic lips. The dynamics of a beam can be the results of air being projected from different areas of the lips. Furthermore, the shape of the different air sacs can be manipulated by different degrees of inflation to highly affect the shape of the beam. These factors were not considered by Kloepper *et al.* (2012) and Kloepper *et al.* (2015), thus the ideas in the studies are not tenable.

It also should be noted that the results in this study only represent the vertical biosonar beam, the roles of structures could be a little different in the horizontal plane during the emission. Since the reflection effects from the rostrum are mainly in the vertical plane, the air sacs (have large acoustic impedance mismatch to the surrounding soft tissues) and soft tissues in the forehead such as the melon and connective tissue could be important contributors to form the horizontal beam.

IV. CONCLUSIONS

In this study an exponentially damped sinusoidal signal was used to model the driving source produced by the phonic lips rapidly opening and closing as pressurized air created a vibration which ultimately produced the echolocation clicks that are emitted into the water. The propagation of clicks in the head of harbor porpoise in the vertical plane was investigated by performing a numerical simulation. The model was set up based on the high resolution CT scans data. In the vertical plane, the properties of the beam pattern in the far field and the waveforms of the receiving points around the forehead were compared with prior measurement results, the simulation results were consistent with the measurement results from the same species but different individuals with different head sizes and different species.

The role of the main structures in the head such as the air sacs, melon and skull in the acoustic propagation was investigated. Additionally, the study provided the first visual evidence of the role of the melon in the sound propagation processes by calculating the beam patterns and sound pressure at four positions when the sound travelled through the melon. The results suggested that reflections off the air sacs and skull in the dolphin's head were the major contributors to the formation of the vertical biosonar beam. The melon is an important structure which fills a large proportion of the forehead and its main role may be as a collimator or acoustic waveguide, but also providing slight narrowing of the resultant biosonar beam and as an impedance transformer providing an impedance transition from deep within the animal's head to sea water. The study presented an effective method to gain better understanding the physiological mechanisms of the sound propagation in the heads of odontocetes.

Adam, O., Cazau, D., Gandilhon, N., Fabre, B., Laitman, J. T., and Reidenberg, J. S. (**2013**). "New acoustic model for humpback whale sound production," Appl. Acoust. **74**, 1182–1190.

Aroyan, J. L. (**2001**). "Three-dimensional modeling of hearing in *Delphinus delphis*," J. Acoust. Soc. Am. **110**(6), 3305–3318.

Aroyan, J. L., Cranford, T. W., Kent, J., and Norris, K. S. (**1992**). "Computer modeling of acoustic beam formation in *Delphinus delphis*," J. Acoust. Soc. Am. **92**(5), 2539–2545.

Au, W. W. L. (**1993**). *The Sonar of Dolphins* (Springer-Verlag, New York), 277 pp.

Au, W. W. L., and Hastings, M. (**2008**). *Principles of Marine Bioacoustics* (Springer-Verlag, New York).

Au, W. W. L., Houser, D. S., Finneran, J. J., Lee, W., Talmadge, L. A., and Moore, P. W. (**2010**). "The acoustic field on the forehead of echolocating Atlantic bottlenose dolphins (*Tursiops truncatus*)," J. Acoust. Soc. Am. **128**(3), 1426–1434.

Au, W. W. L., Kastelein, R. A., and Benoit-Bird, K. J. (**2006**). "Acoustic radiation from the head of echolocating harbor porpoise (*Phocoena phocoena*)," J. Exp. Biol. **209**(14), 2726–2733.

Au, W. W. L., Kastelein, R. A., Rippe, T., and Schooneman, N. M. (**1999**). "Transmission beam pattern and echolocation signals of a harbor porpoise (*Phocoena phocoena*)," J. Acoust. Soc. Am. **106**(6), 3699–3705.

Au, W. W. L., Pawloski, J. L., Nachtigall, P. E., Blonz, M., and Gisner, R. C. (**1995**). "Echolocation signals and transmission beam pattern of a false killer whale (*Pseudorca crassidens*)," J. Acoust. Soc. Am. **98**(1), 51–59.

Bérenger, J. P. (**1994**). "A perfectly matched layer for the absorption of electromagnetic waves," J. Comput. Phys. **114**(2), 185–200.

Cranford, T. W. (**1988**). "Anatomy of acoustic structures in the spinner dolphin forehead as shown by x-ray computed tomography and computer graphics," in *Animal Sonar: Processes and Performance*, edited by P. E. Nachtigall and P. W. B. Moore (Plenum Publishing Co., New York), pp. 67–77.

Cranford, T. W. (**1992**). "Functional morphology of the odontocete forehead: Implications for sound generation," Ph.D. thesis, The University of California, Santa Cruz, CA.

Cranford, T. W. (**2000**). "In search of impulse sound sources in odontocetes," in *Hearing by Whales and Dolphins*, edited by W. W. L. Au, A. N. Popper, and R. R. Fay (Springer-Verlag, New York), pp. 109–156.

Cranford, T. W., Amundin, M., and Norris, K. S. (**1996**). "Functional morphology and homology in the odontocete nasal complex: Implications for sound Generation," J. Morphol. **228**, 223–285.

Cranford, T. W., Trijoulet, V., Smith, C. R., and Krysl, P. (**2014**). "Validation of a vibroacoustic finite element model using bottlenose dolphin simulations: The dolphin biosonar beam is focused in stages," Bioacoustics **23**(2), 161–194.

Duck, F. A. (**1990**). *Physical Properties of Tissue: A Comprehensive Reference Book* (Academic Press, San Diego, CA).

Finneran, J. J., Branstetter, B. K., Houser, D. S., Moore, P. W., Mulsow, J., Martin, C., and Perisho, S. (**2014**). "High-resolution measurement of a bottlenose dolphin's (*Tursiops truncatus*) biosonar transmission beam pattern in the horizontal plane," J. Acoust. Soc. Am. **136**(4), 2025–2038.

Finneran, J. J., Mulsow, J., Branstetter, B. K., Moore, P. W., and Houser, D. S. (**2016**). "Nearfield and farfield measurements of dolphin echolocation beam patterns: No evidence of focusing," J. Acoust. Soc. Am. **140**(2), 1346–1360.

Goodson, A. D., Kastelein, R. A., and Sturtivant, C. R. (**1995**). "Source levels and echolocation signal characteristics of juvenile harbour porpoises (*Phocoena phocoena*)," in *Harbour Porpoise: Laboratory Studies to Reduce Bycatch*, edited by P. E. Nachtigall, J. Lien, W. W. L. Au, and A. J. Read (De Spil, Woerden, the Netherlands), pp. 41–53.

Hatakeyama, Y., and Soeda, H. (**1990**). "Studies on echolocation of porpoises taken in salmon gillnet fisheries," in *Sensory Abilities of Cetaceans*, edited by J. A. Thomas and R. A. Kastelein (Springer-Verlag, New York), pp. 269–281.

Houser, D. S., Finneran, J. J., Carder, D. A., Van Bonn, W., Smith, C., Hoh, C., Mattrey, R., and Ridgway, S. H. (**2004**). "Structural and functional imaging of bottlenose dolphin (*Tursiops truncatus*) cranial anatomy," J. Exp. Biol. **207**, 3657–3665.

Huggenberger, S., Rauschmann, A. M., Vogl, J. T., and Oelschlager, H. H. H. (**2009**). "Functional morphology of the nasal complex in the Harbor porpoise (*Phocoena phocoena L.*)," Anatomical Record **292**, 902–920.

Kamminga, C., and Wiersma, H. (**1981**). "Investigations on cetacean sonar II. Acoustical similarities and differences in odontocete sonar signals," Aquat. Mamm. **8**, 41–62.

Karol, C., Litchfield, C., Caldwell, D. K., and Caldwell, M. C. (**1978**). "Compositional topography of melon and spermaceti organ lipids in the pygmy sperm whale (*Kogia breviceps*): Implications for echolocation," Mar. Biol. **47**(2), 115–123.

Kloepper, L., Buck, J. R., Smith, A. B., Supin, A. Y., Gaudette, J. E., and Nachtigall, P. E. (**2015**). "Support for the beam focusing hypothesis in the false killer whale," J. Exp. Biol. **218**(15), 2455–2462.

Kloepper, L., Nachtigall, P. E., Donahue, M. J., and Breese, M. (**2012**). "Active echolocation beam focusing in the false killer whale, *Pseudorca crassidens*," J. Exp. Biol. **215**(8), 1306–1312.

Koblitz, J. C., Wahlberg, M., Stilz, P., Madsen, P. T., Beedholm, K., and Schnitzler, H. (**2012**). "Asymmetry and dynamics of a narrow sonar beam in an echolocating harbor porpoise," J. Acoust. Soc. Am. **131**(3), 2315–2324.

Møhl, B., and Andersen, S. (**1973**). "Echolocation: High-frequency component in the click of the harbor porpoise (*Phocoena ph. L.*)," J. Acoust. Soc. Am. **54**(5), 1368–1372.

Moore, P. W., Dankiewicz, L. A., and Houser, D. S. (**2008**). "Beamwidth control and angular target detection in an echolocating bottlenose dolphin (*Tursiops truncatus*)," J. Acoust. Soc. Am. **124**(5), 3324–3332.

Morris, R. J. (**1986**). "The acoustic faculty of dolphins," in *Research on Dolphins*, edited by M. M. Bryden and R. J. Harrison (Clarendon Press, New York), pp. 369–399.

Nakamura, K., Yamada, T. K., and Shimazaki, K. (**1998**). "Measurements of the nasal sacs of individual common dolphin, *Delphinus delphis*, and Dall's porpoise, *Phocoenoides dalli*, by means of silicon reconstruction," Mamm. Study **23**, 119–122.

Soldevilla, M. S., McKenna, M. F., Wiggins, S. M., Shadwick, R. E., Cranford, T. W., and Hildebrand, J. A. (**2005**). "Cuvier's beaked whale (*Ziphius cavirostris*) head tissues: Physical properties and CT imaging," J. Exp. Biol. **208**(12), 2319–2332.

Song, Z., Zhang, Y., Berggren, P., and Wei, C. (**2017**). "Reconstruction of the forehead acoustic properties in an Indo-Pacific humpback dolphin (*Sousa chinensis*), with investigation on the responses of soft tissue sound velocity to temperature," J. Acoust. Soc. Am. **141**(2), 681–689.

Song, Z., Zhang, Y., Wei, C., and Wang, X. (**2016**). "Inducing rostrum interfacial waves by fluid-solid coupling in a Chinese river dolphin (*Lipotes vexillifer*)," Phys. Rev. E **93**, 012411.

Wei, C., Au, W. W. L., Song, Z., and Yu, Z. (**2016**). "The role of various structures in the head on the formation of the biosonar beam of the baiji (*Lipotes vexillifer*)," J. Acoust. Soc. Am. **139**(2), 875–880.

Wei, C., Wang, X., Song, Z., Li, L., Zhang, Y., Zhu, Q., Liang, K., and Ye, F. (**2013**). "Sound velocity distribution reconstruction of an Indo-Pacific humpback dolphin's head based on CT scan," Tech. Acoust. **32**(5), 34–36.

Wei, C., Wang, Z., Song, Z., Wang, K., Wang, D., Au, W. W. L., and Yu, Z. (**2015**). "Acoustic property reconstruction of a neonate Yangtze finless porpoise's (*Neophocaena asiaeorientalis*) head based on CT imaging," PLoS One **10**(4), e0121442.

Wei, C., Yu, Z., and Au, W. W. L. (**2014**). "Simulation of ultrasound beam formation of baiji (*Lipotes vexillifer*) with a finite element model," J. Acoust. Soc. Am. **136**(1), 423–429.

Wisniewska, D. M., Johnson, M., Beedholm, K., Wahlberg, M., and Madsen, P. T. (**2012**). "Acoustic gaze adjustments during active target selection in echolocating porpoises," J. Exp. Biol. **215**(24), 4358–4373.

Wisniewska, D. M., Ratcliffe, J. M., Beedholm, K., Christensen, C. B., Johnson, M., Koblitz, J. C., Wahlberg, M., and Madsen, P. T. (**2015**). "Range-dependent flexibility in the acoustic field of view of echolocating porpoises (*Phocoena phocoena*)," eLife **4**, e05651.